ADVANCED MATERIALS

DOI: 10.1002/adma.200701798

Evidence of Large Voids in Pure-Silica-Zeolite Low-*k* Dielectrics Synthesized by Spin-on of Nanoparticle Suspensions**

By *Salvador Eslava, Mikhail R. Baklanov,* Alexander V. Neimark, Francesca Iacopi, Christine E. A. Kirschhock, Karen Maex,* and *Johan A. Martens**

The downscaling of feature sizes in integrated circuits (IC) requires on-chip interconnects with low dielectric constant layers (low-*k*) that mitigate the increase in propagation delay and power consumption.[1–4] Several candidate low-*k* materials based on porous silicates have been proposed.[1–4] Whereas porosity is beneficial for lowering the dielectric constant, it has detrimental effects on the mechanical properties of the layer, strongly complicating the integration process of the on-chip interconnects.[2] In addition to a low dielectric constant and sufficient mechanical strength, the pores in dielectric layers need to be narrow (<5 nm)[5] and uniform to permit a proper sealing that avoids electrical breakdowns resulting from diffusion of Cu and other conducting species.[1–4] Dielectric layers that consist of pure-silica zeolite (PSZ) prepared by in situ crystallization seem to be outstanding, as they achieve high elastic moduli in combination with low *k* values and, moreover, pores are reported to be hardly 0.5 nm wide.[3,4,6,7] High stiffness results from the crystalline nature of the zeolite.[7] Silicalite-1 (i.e., PSZ with MFI framework topology) is a commonly investigated zeolite.[7] By spin-on deposition of a suspension of Silicalite-1 nanocrystals together with residual silica from the synthesis, a layer with a bimodal pore size distribution (PSD) is obtained, comprising zeolite channels with diameters of ca. 0.5 nm and interstitial voids with diameters smaller than 4 nm located between the Silicalite-1 nanocrystals.[8–10] This bimodal pore model has been adopted in several studies and reviews.[3,4,7–17] With Silicalite-1, ultralow *k* values ($k < 2.4$) can be achieved for the highest ever reported elastic moduli.[3] We investigated these Silicalite-1 layers and found that larger voids of a few tens of nanometers wide are present. We demonstrate that these large voids are always present when the *k* value is lower than 3.

In literature, the PSD of Silicalite-1 films was estimated based on the analysis of nitrogen adsorption isotherms on powdery Silicalite–1 product that was processed in a similar way as the film.[8–10] The isotherms typically show a low pressure uptake in micropores and adsorption in the region $P/P_0 = 0.85–1$,[8,10] which reveals the presence of mesopores. The isotherms show hysteresis and a sudden nitrogen desorption in the relative pressure range 0.40–0.50, which has been interpreted in terms of capillary desorption from pores with diameters of 2.6–4 nm.[8–10] These pore diameters were estimated using Barrett–Joyner–Halenda (BJH) method.[8–10] Isotherms presenting such sudden nitrogen desorption at P/P_0 values in the range 0.40–0.50 must be interpreted with caution, since the desorption may be related to a cavitation phenomenon rather than capillary desorption.[18–25] As the PSD in low-*k* materials is one of the critical properties, we decided to make a comparative investigation of porosities of Silicalite-1 films and the corresponding powders subjected to a similar drying and calcination procedure. Powdery Silicalite-1 was characterized by using nitrogen adsorption, and the films by using ellipsometric porosimetry.

Silicalite-1 was synthesized from clear solution, as described elsewhere.[8] During this synthesis, the silica is present as oligomers, preorganized nanoparticles measuring ca. 4 nm, and Silicalite-1 nanocrystals.[26–35] The Silicalite-1 grows by aggregation of the preorganized nanoparticles.[26–35] The Silicalite-1 crystallization time was varied from 3 to 5 days in order to alter the proportion of Silicalite-1 nanocrystals to residual silica in the suspension. The Silicalite-1 nanocrystal average size increased from 40 to 66 nm with prolongation of the crystallization (Fig. 1). The nanocrystal content on silica basis, determined by ultracentrifugation, increased from 6 wt % after 3 days to ca. 60 wt % after 5 days (Fig. 1). In the period from 3 to 5 days the Silicalite-1 nanocrystal content increased by growth of existing nanocrystals and formation of additional ones.[33,34]

To simulate the spin on Silicalite-1 film as previously done in literature,[8–10] samples of Silicalite-1 suspensions were dried and calcinated. Nitrogen and argon adsorption isotherms were determined at −196 °C on this powdery Silicalite-1 (Fig. 2).

[*] Dr. M. R. Baklanov, S. Eslava, Dr. F. Iacopi, Prof. K. Maex[+]
Interuniversitary MicroElectronic Center (IMEC)
Kapeldreef 75, 3001 Leuven (Belgium)
E-mail: baklanov@imec.be
Prof. J. A. Martens, S. Eslava, Prof. C. E. A. Kirschhock
Centrum voor Oppervlaktechemie en Katalyse
Katholieke Universiteit Leuven
Kasteelpark Arenberg 23, 3001 Leuven (Belgium)
E-mail: johan.martens@biw.kuleuven.be
Prof. A. V. Neimark
Department of Chemical and Biochemical Engineering, Rutgers
The State University of New Jersey
98 Brett Road, Piscataway, NJ 08854-8058 (USA)

[+] Present address: Department of Electrical Engineering (ESAT-INSYS), Katholieke Universiteit Leuven, Kasteelpark Arenberg 10, 3001 Leuven, Belgium.

[**] We thank Dr. A. Aerts for scientific discussions on nitrogen adsorption. C.E.A.K. and J.A.M. acknowledge the Flemish government for a concerted research action (GOA).

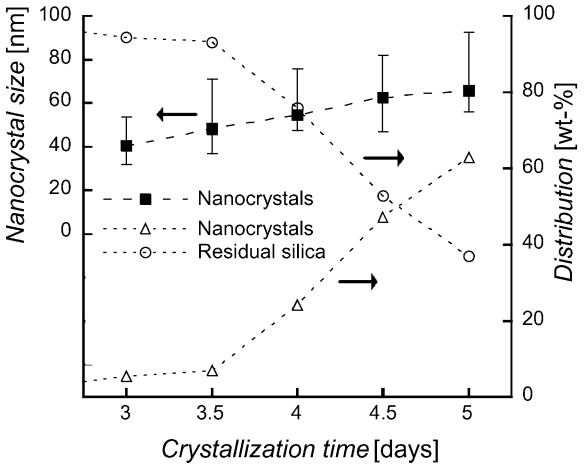

Figure 1. Characteristics of Silicalite-1 suspensions after different crystallization times.

The nitrogen adsorption isotherms of these Silicalite-1 powders are in agreement with previously published data on similarly prepared samples.[8,10] The sample obtained from Silicalite-1 suspension crystallized for 3 days shows a type I isotherm typical of a microporous material.[18] From the absence of mesopores it appears that in this material, the relatively small amount of nanocrystals and the abundant amount of residual silica (Fig. 1) together are closely packed, leaving microporous interstitial voids only. Prolongation of the crystallization leads to samples with enhanced nitrogen adsorption capacity (Fig. 2). In the Silicalite-1 products obtained after 4.5 and 5 days of crystallization, there is a significant rise of the nitrogen adsorption isotherm near the saturation pressure (Fig. 2a). This uptake is ascribed to capillary condensation of nitrogen in mesoscale interstitial cavities between packed nanocrystals. In these longer-crystallized Silicalite-1 suspensions, the larger relative concentration of nanocrystals (Fig. 1) explains the formation of interstitial voids upon aggregation during the drying and calcination processes.

Analysis of adsorption isotherms of two different molecular probes is a proven approach to discriminate between capillary desorption and cavitation.[22] The nitrogen adsorption isotherms present significant hysteresis and close abruptly at P/P_0 of ca. 0.5 (Fig. 2a). The argon adsorption isotherms of the Silicalite-1 samples crystallized for 4.5 and 5 days show hysteresis loops with abrupt argon desorption at a relative pressure of ca. 0.35 (Fig. 2b). This sudden desorption of nitrogen and argon at the characteristic relative pressures around 0.50 for nitrogen and around 0.35 for argon have been attributed to cavitation in many experimental studies and simulations.[20–23] These relative pressures would correspond to the non-overlapping ranges of pore sizes 5–6 nm (nitrogen desorption isotherm) and 4–5 nm (argon desorption isotherm), estimated using the nonlocal density functional theory (NLDFT) method for equilibrium desorption.[22] This discrepancy further substantiates the occurrence of cavitation rather than capillary desorption.

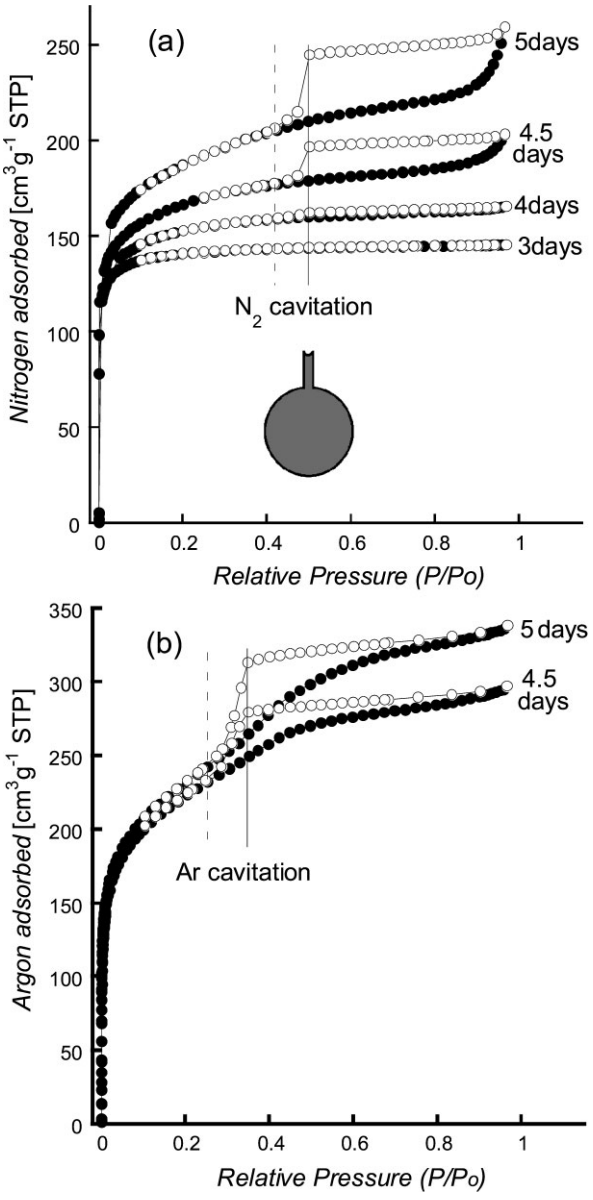

Figure 2. Nitrogen (a) and argon (b) adsorption (●)–desorption (○) isotherms at −196 °C up to $P/P_0 = 0.97$ on calcined zeolite product used to prepare spin-on Silicalite-1 low-*k* films. The Silicalite-1 crystallization time is indicated. The vertical solid and dashed lines indicate the cavitation pressure and the lower closure point of the hysteresis loops, respectively. The inset in (a) is a drawing of an ink-bottle pore.

Cavitation usually occurs in adsorbents with a network of ink-bottle pores, which represent voids connected to the external surface by narrow necks (sketched in the inset in Fig. 2a).[18–25] In ink-bottle pores, the wide cavities are filled with condensate at high relative pressures. Pore emptying during desorption is hindered, because the meniscus in the necks is strongly curved and prevents evaporation. Because the tensile strength of the liquid adsorbate that is condensed in the ink-bottle pores has a maximum limit, there exists a specific vapor pressure below which the capillary condensed liquid can

ADVANCED MATERIALS

no longer withstand the tension and disintegrates. The relative pressure at which cavitation occurs determines the lower limit of the neck sizes that can be assessed in the desorption experiment. In ink-bottle pores with necks that are smaller than this critical diameter, desorption is initiated by cavitation, and the pressure of desorption does not depend on the neck size. Thus, ignoring cavitation effects and using the standard BJH method for calculating the PSD lead to artificial predictions of pores with diameters of about 4 nm. Note that the values of pore sizes estimated by the standard BJH methods are smaller than those predicted by the NLDFT method by approximately 1 nm in the given range of pore sizes. In this situation, the adsorption branch provides reliable information on the size of body of the cavities.[18,22,24,25]

The cavity sizes were estimated from the adsorption branches of the nitrogen adsorption isotherms by using the hybrid NLDFT for cage-like silica materials.[20,22] This method implies that the pore system is represented as a 3D network of spherical cavities of diameters larger than 5 nm connected by cylindrical channels with diameters smaller than 5 nm. In the region of hysteresis, it is assumed that the pore filling along the adsorption branch occurs via the mechanism of delayed condensation. It was shown that this model provides a reasonable description of micro- and mesoporous silica materials with cage-like pores.[22] The PSDs in the ranges 2–35 nm and 5–35 nm are given in Figure 3. The pore width of the majority of mesopores is in the range 2–5 nm. The sample crystallized for 3 days contains only a very small amount of pores in this size range, in agreement with the type I adsorption isotherm of this sample (Fig. 2a). Longer crystallization leads to the formation of more cavities measuring 2–5 nm (Fig. 3a), as well as of larger ones with sizes up to 35 nm albeit in smaller quantities (Fig. 3b). The volume percentage of mesopores wider than 5 nm in the totality of mesopores is presented in Figure 4. According to the assumed model, these wide cavities are connected to the exterior by narrow micro- and mesopores necks with diameters smaller than 5 nm. Note that in order to probe the presence of cavities wider than 35 nm, the adsorption isotherms should be recorded at relative pressures P/P_0 higher than 0.97 used here. At such pressures, the accuracy of the measurement and the application of the Kelvin equation for estimating mesopore sizes become problematic.

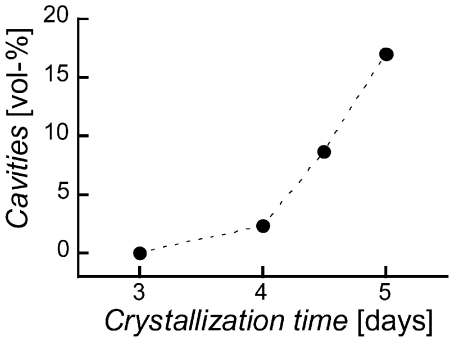

Figure 4. Volume percentage of pores wider than 5 nm in the 2–35 nm pores in Silicalite-1 powder as a function of the crystallization time of the Silicalite-1 suspension (data from Fig. 3).

The ink-bottle-pore shape for these Silicalite-1 samples deduced from the sorption experiments can be understood as follows. The suspension comprises Silicalite-1 nanocrystals and residual silica. The latter is mainly present as pre-organized silica nanoparticles of ca. 4 nm.[26–35] Nanocrystals and nanoparticles build a 3D network, as schematically represented in Figure 5. The filling of voids between nanocrystals depends on the ratio of silica nanoparticles to Silicalite-1 nanocrystals (Fig. 2). The powder obtained after 3 days crystallization has micropores only, suggesting that there were enough silica nanoparticles to fill all interstitial spaces (Fig. 5a). In later samples, having a larger content of Silicalite-1 nanocrystals, the content of residual silica is insufficient to fill all interstitial voids (Fig. 5b). Thus, relatively large voids between the nanocrystals are formed and probed with nitrogen adsorption (Fig. 3b).

The nitrogen adsorption isotherms provide information on the porosity of powdery Silicalite-1 products, which may differ from the actual films. We used ellipsometric porosimetry (EP) to evaluate the on-wafer porosity and compare with the observations on the powders.[37,38] EP is equally based on the

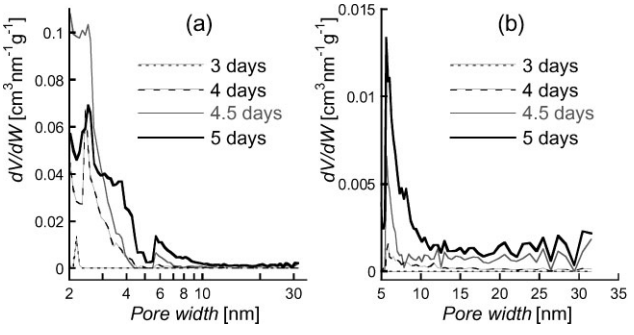

Figure 3. Pore size distribution for the calcined zeolite product used to prepare spin-on Silicalite-1 films, and calculated from the adsorption branches of the nitrogen isotherms of Figure 2a. The PSD in the pore size range 2–35 nm is shown in (a); the PSD in the pore size range 5–35 nm is expanded in (b).

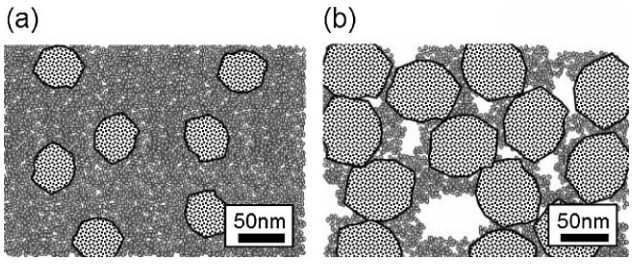

Figure 5. Sketch of Silicalite-1 products consisting of Silicalite-1 nanocrystals and residual nanoparticles for a relatively short (a) and long (b) crystallization time. Nanocrystals measure ca. 40 nm in (a) and ca. 66 nm in (b); nanoparticles measure ca. 4 nm. Nanocrystal shape is based on TEM investigations published elsewhere. [36]

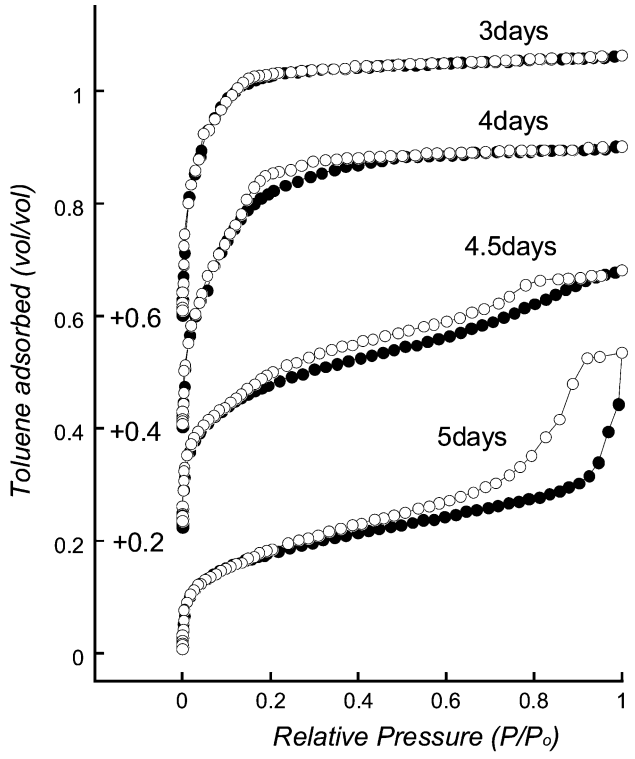

Figure 6. Toluene adsorption (●)-desorption (○) isotherms at 20 °C on spin-on Silicalite-1 films prepared with different crystallization times. The Silicalite-1 crystallization time is indicated. Isotherms measured by EP at 633 nm wavelength. Distributions have been shifted vertically for clarity.

analysis of adsorption isotherms of toluene or other molecular probes but the isotherms are obtained via spectroscopic ellipsometry.[37,38] Figure 6 shows the toluene adsorption isotherms on the calcined films prepared by spinning on the Silicalite-1 suspensions on top of silicon wafers. For each crystallization time, the adsorption isotherm of toluene on the Silicalite-1 film (Fig. 6) and of nitrogen and argon on the corresponding powdery Silicalite-1 product (Fig. 2) reveal a similar pore structure. PSZ films and powders after 3 and 5 days of crystallization are taken as examples. For 3 days of crystallization, EP using toluene (Fig. 6) and nitrogen adsorption (Fig. 2a) show a type I isotherm typical of a microporous system. For Silicalite-1 preparations involving 5 days of crystallization, EP (Fig. 6) reveals toluene adsorption over the whole range of relative pressures and significant hysteresis. A similar isotherm with hysteresis is recorded upon nitrogen and argon adsorption on the powder (Fig. 2).

For samples with 4.5 and 5 days of crystallization, the toluene adsorption isotherms of Figure 6 reveal the presence of relatively large voids probed by sorbate uptake at high relative pressures.[24,25] In powdery samples, the large voids are emptied first by capillary desorption and finally by cavitation as already discussed. The relative pressure at which cavitation occurs for toluene is ca. 0.2 at 20 °C, corresponding to a critical diameter ca. 3.2 nm.[39] During toluene desorption from the 4.5 and 5 day films (Fig. 6), there is no capillary condensed toluene remaining at this critical relative pressure (Fig. 6). Then, capillary desorption is the main toluene evacuation mechanism.

The PSD of the films in the range 2–100 nm was derived from the toluene adsorption and desorption isotherms by using a standard model based on the Kelvin equation, as previously published elsewhere (Fig. 7).[37] This model has been demonstrated to yield data in good agreement with other techniques.[40] Note that the model is less accurate for larger mesopores (larger than 20 nm). For 20–100 nm wide pores, the standard deviation is estimated at ~10 nm. The PSDs derived from adsorption and desorption branches are in rather good agreement, except for the largest pores in the samples crystallized from 4.5 days on (Fig. 7). All films contain mesopores measuring 2–5 nm and the most crystallized films (4.5 and 5 days) contain a significant amount of wider pores. In those cases where large mesopores are present, the PSDs show much larger values calculated from the adsorption than from the desorption isotherms (Fig. 7). In 4.5-days film, the widths are 3 times larger in the adsorption analysis. In 5-days film, the ratio cannot be calculated because of the upper limit at 100 nm. These differences in the PSD between the adsorption and desorption analysis are characteristic of the presence of large cavities interconnected by smaller necks.[18–25] In this case, the analysis in the adsorption branch estimates the size of the widest parts of the cavities, the desorption branches the narrowest parts.[18,22,24,25] The wide cavities are distributed up to 80 nm in 4.5-days film and up to at least 100 nm in 5-days film.

Powders and films prepared from Silicalite-1 crystallized for 4.5 and 5 days both contain voids that are wider than 5 nm (Figs. 3 and 7). The cavity size in films extends even beyond the upper limit of the mesoporous range (2–50 nm). In the films the pore restrictions are also wider than in the powders. One can

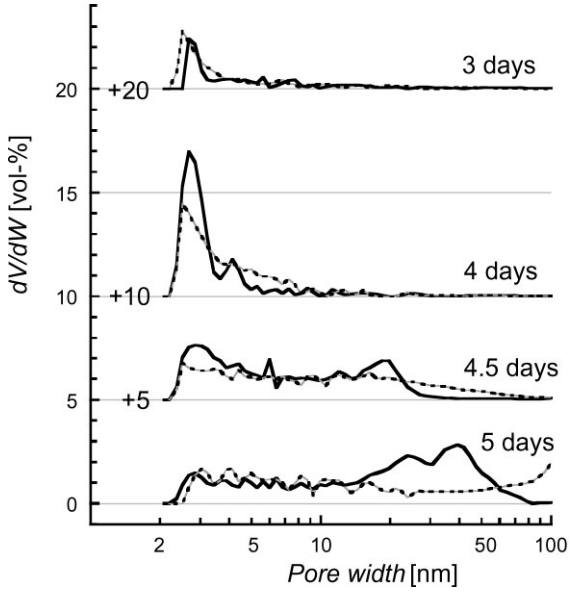

Figure 7. PSD on spin-on Silicalite-1 films calculated from the adsorption branches (dashed line) and desorption branches (solid line) of the toluene isotherms of Figure 6. Distributions have been shifted vertically for clarity.

ADVANCED MATERIALS

speculate about the reason for this. First, the interstitial cavities may remain open because their size approaches that of the film thickness (380–480 nm). Second, there is a different stress during the drying of the nanocrystals powder and a thin film. Differences in the calcination procedure can also have some impact. The films were calcined at 450 °C because this temperature was sufficient to remove the organic template. However, the powdery product needed up to 600 °C to evacuate the organic template. Similar differences in temperature needed for processing films and powdery Silicalite-1 product were previously reported.[10]

The characterization of powders and films leads to the interpretation of the porosities as sketched in Figure 5. The only difference is that in films the percolation in the pore structure is not controlled by very narrow necks. For long crystallizations the cavities were measured by nitrogen adsorption to be at least 35 nm wide. Toluene adsorption analysis confirms the presence of such wide cavities and evidences the existence of even larger ones (Fig. 7). Actually, the large cavities have a size comparable to the nanocrystal size, that is, tens of nanometers as sketched in Figure 5. High-resolution scanning electron microscopy (SEM) on a cross section of the film with 5 days of crystallization confirms the presence of holes of such dimensions (Fig. 8).

A bimodal pore size distribution with micropores ca. 0.5 nm and mesopores smaller than 4 nm was adopted in many studies on spin-on Silicalite-1 films.[3,4,7–17] Some films were characterized using positronium annihilation lifetime spectroscopy (PALS).[12,14–16] In PALS the dynamic range of the pore-size measurement extends from sub-nanometers up to 30 nm.[41–43] In literature, films were sealed to avoid the escape and annihilation of the positronium (Ps) in the vacuum and thus fulfill a necessary requirement in PALS to measure the intrinsic pore size.[12] Despite the sealing, the Ps intensity in vacuum was still ca. 30%.[12] This was originally attributed to backscattering. An alternative explanation based on the present work is that there was annihilation of Ps in large cavities. Note that it is not possible to distinguish the lifetime of Ps annihilating in vacuum from that in voids larger than 30 nm.

The evolution of the *k*-value and the porosity with the Silicalite-1 nanocrystal content of spin-on Silicalite-1 films is shown in Figure 9. The volume percentage of cavities is calculated from the analysis of the toluene adsorption isotherm

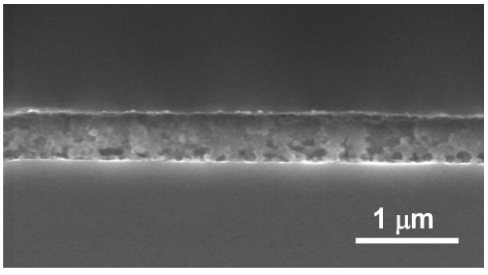

Figure 8. High-resolution SEM image of a cross section of the spin-on Silicalite-1 film with a crystallization time of 5 days (scale bar: 1 μm).

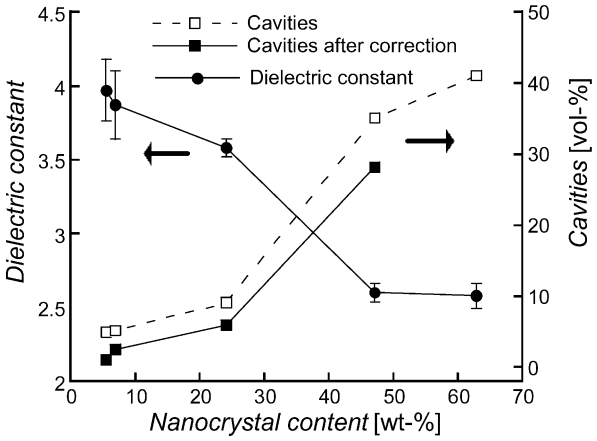

Figure 9. Dielectric constant and the volume percentage of cavities proved to be larger than 5 nm within the films as a function of the nanocrystal content of the Silicalite-1 suspension used to deposit the film. The deviation in the porosity calculation due to swelling is corrected up to 4.5 days of crystallization (solid lines).

branches (Fig. 6). A correction for swelling is made based on the measured refractive index during the adsorption isotherms (solid line in Fig. 9). The percentage of cavities for the film with 5 days of crystallization could not be corrected for the swelling because of the difficult fitting during the abrupt toluene adsorption on the large voids. Figure 9 shows that the dielectric constant decreases with the nanocrystal content. The decrease in dielectric constant results in part from the higher crystallinity of films with higher nanocrystal content. More crystalline films offer less polar hydroxyls and thus, the dielectric constant is decreased.[10] Second, the reduction in dielectric constant is due to the increase in porosity with increasing nanocrystal content, viz. ca. 10% from 3 to 5 days of crystallization (Fig. 6). Thus, low dielectric constant values ($k < 3$) are obtained in films with a substantial amount of wide cavities. This reveals that any increase of the crystallinity by increasing the content of 40–100 nm nanocrystals, as proposed elsewhere to decrease the dielectric constant,[10] yields films with more embedded large voids because of the lack of residual silica that can effectively fill the interstitial voids between the nanocrystals.

In conclusion, spin-on Silicalite-1 low-*k* films, prepared following published procedures in which zeolite nanocrystals are embedded in a precursor silica matrix,[8–10] possess not only 0.55 nm Silicalite-1 micropores but also embedded voids of 2–5 nm and larger cavities in the range of tens of nanometers. The formation of cavities in the film occurs provided the content of residual silica from the synthesis does not suffice to fill the voids left between nanocrystals measuring 40–70 nm. The higher the nanocrystal content (and thus the crystallinity) of the suspension employed for spin-on, the larger the amount of embedded large voids. Thus, spin-on Silicalite-1 films with *k* values below 3 contain a population of pores in the range of few tens of nanometers. The difficulty of sealing these wide voids represents a considerable and exciting challenge in the implementation of spin-on Silicalite-1 films as low-*k* dielectrics.

Finally, we anticipate that the same properties are characteristic of other spin-on zeolite low-*k* films produced from zeolite nanocrystals dispersed in a precursor silica material (e.g., MEL[44,45]).

Experimental

Zeolite suspensions were prepared following the procedure of Wang et al. [8]. First, a clear precursor sol (clear solution) was prepared by mixing tetraethyl-orthosilicate (TEOS), aqueous tetrapropylammonium hydroxide (TPAOH), and ethanol (EtOH) with a final molar ratio of $2.8SiO_2$/40water/22.4EtOH/1TPAOH in an autoclavable polypropylene bottle. The clear solution was stirred for 3 days, slowly heated up to 80 °C in an oil bath, and kept for 5 days. Samples were withdrawn at different crystallization times from 3 to 5 days. Every nanoparticle suspension was centrifuged at 5000 rpm for 30 min and filtered through 200 nm PTFE filters to remove large nanoparticles. Silicalite-1 products were prepared by drying and calcining the as-filtered suspensions in air at 80 °C and 600 °C, respectively. To calculate the nanocrystal content, each suspension was diluted with water (×5) to lower the viscosity and then centrifuged at 18000 rpm for 2.5 h at 20 °C. The deposited nanocrystals were recovered in ethanol, calcined in air at 600 °C for 5 h, and weighted. The supernatant liquid was also calcined under identical conditions and weighted. Then, the nanocrystal weight percentage was calculated on a silica basis. Particle-size analysis was carried out by dynamic light scattering (DLS) on an ALV-NIBS high performance particle sizer, and corrected for variation in viscosity by using a viscometer (AMVn Anton Paar). Nitrogen and argon adsorption isotherms were recorded at −196 °C by using a Micromeritics Tristar 3000 on zeolite products degassed at 300 °C for 10 h in nitrogen flow. Silicalite-1 suspensions were spun both onto pieces of Si-p wafer for ellipsometric measurements and onto pieces of Si-n^{++} wafers for capacitance measurements. The velocity used was 3300 rpm for 30 s and the acceleration was 1300 rpm s^{-1}. The films were dried at 80 °C overnight and calcined in air at 450 °C for 2.5 h. Toluene adsorption isotherms were obtained by monitoring the ellipsometric angles Ψ and Δ at 633 nm wavelength during the adsorption and desorption (ellipsometric porosimetry with a ellipsometer Sentech SE801). In parallel, the thickness and refractive index were measured by using the collected spectra of Ψ and Δ in the region 350–850 nm. Further details of the ellipsometric porosimetry characterization were previously published elsewhere by some of us [37,38]. The dielectric constant in the calcined film was measured after degassing at 150 °C in nitrogen flow in a MIS-type capacitor obtained by deposition of Al dots on top of the films. Cross-section images of Silicalite-1 films were obtained by scanning electron microscopy (SEM, W-filament, Philips X-30, 5 kv).

Received: July 23, 2007
Revised: December 20, 2007
Published online: June 16, 2008

[1] K. Maex, M. R. Baklanov, D. Shamiryan, F. Iacopi, S. H. Brongersma, Z. S. Yanovitskaya, *J. Appl. Phys.* **2003**, *93*, 8793.
[2] M. R. Baklanov, K. Maex, *Philos. Trans. R. Soc. London Ser. A* **2006**, *364*, 201.
[3] G. Dubois, R. D. Miller, W. Volksen, in *Dielectric Films for Advanced Microelectronics*, (Eds: M. R. Baklanov, M. Green, K. Maex), Wiley, Chichester, UK **2007**, Ch. 2.
[4] B. D. Hatton, K. Landskron, W. J. Hunks, M. R. Bennett, D. Shukaris, D. D. Perovic, G. A. Ozin, *Mater. Today* **2006**, *9*(3), 22.
[5] M. H. Ree, J. W. Yoon, K. Y. Heo, *J. Mater. Chem.* **2006**, *16*, 685.
[6] Z. B. Wang, H. T. Wang, A. P. Mitra, L. M. Huang, Y. S. Yan, *Adv. Mater.* **2001**, *13*, 746.
[7] Z. J. Li, M. C. Johnson, M. W. Sun, E. T. Ryan, D. J. Earl, W. Maichen, J. I. Martin, S. Li, C. M. Lew, J. Wang, M. W. Deem, M. E. Davis, Y. S. Yan, *Angew. Chem. Int. Ed.* **2006**, *45*, 6329.
[8] Z. B. Wang, A. P. Mitra, H. T. Wang, L. M. Huang, Y. S. Yan, *Adv. Mater.* **2001**, *13*, 1463.
[9] S. Li, Z. J. Li, Y. S. Yan, *Adv. Mater.* **2003**, *15*, 1528.
[10] Z. J. Li, S. Li, H. M. Luo, Y. S. Yan, *Adv. Funct. Mater.* **2004**, *14*, 1019.
[11] S. Li, Z. J. Li, D. Medina, C. Lew, Y. S. Yan, *Chem. Mater.* **2005**, *17*, 1851.
[12] S. Li, J. N. Sun, Z. J. Li, H. G. Peng, D. Gidley, E. T. Ryan, Y. S. Yan, *J. Phys. Chem. B* **2004**, *108*, 11689.
[13] S. Li, X. Wang, D. Beving, Z. W. Chen, Y. S. Yan, *J. Am. Chem. Soc.* **2004**, *126*, 4122.
[14] H. K. M. Tanaka, T. Kurihara, A. P. Mills, *Phys. Rev. B* **2005**, *72*, 193408.
[15] H. K. M. Tanaka, T. Kurihara, N. Nishiyama, A. P. Mills, *Microporous Mesoporous Mater.* **2006**, *95*, 164.
[16] H. K. M. Tanaka, T. Kurihara, A. P. Mills, *J. Phys. Condens. Matter* **2006**, *18*, 8581.
[17] C. M. Lew, Y. S. Yan, *Stud. Surf. Sci. Catal.* **2007**, *170*, 1502.
[18] S. J. Gregg, K. S. W. Sing, in *Adsorption, Surface Area and Porosity*, 2nd ed., Academic, London **1982**, *Ch. 3 and 4.*
[19] L. Sarkisov, P. A. Monson, *Langmuir* **2001**, *17*, 7600.
[20] P. I. Ravikovitch, A. V. Neimark, *Langmuir* **2002**, *18*, 1550.
[21] P. I. Ravikovitch, A. V. Neimark, *Langmuir* **2002**, *18*, 9830.
[22] M. Thommes, B. Smarsly, M. Groenewolt, P. I. Ravikovitch, A. V. Neimark, *Langmuir* **2006**, *22*, 756.
[23] J. C. Groen, L. A. A. Peffer, J. Perez-Ramirez, *Microporous Mesoporous Mater.* **2003**, *60*, 1.
[24] M. R. Baklanov, K. P. Mogilnikov, J. H. Yim, *Mater. Res. Soc. Symp. Proc.* **2004**, *812*, F5. 4. 1.
[25] J. C. P. Broekhoff, J. H. de Boer, *J. Catal.* **1968**, *10*, 153.
[26] R. Ravishankar, C. E. A. Kirschhock, P. P. Knops-Gerrits, E. J. P. Feijen, P. J. Grobet, P. Vanoppen, F. C. De Schryver, G. Miche, H. Fuess, B. J. Schoeman, P. A. Jacobs, J. A. Martens, *J. Phys. Chem. B* **1999**, *103*, 4960.
[27] C. E. A. Kirschhock, R. Ravishankar, F. Verspeurt, P. J. Grobet, P. A. Jacobs, J. A. Martens, *J. Phys. Chem. B* **1999**, *103*, 4965.
[28] C. E. A. Kirschhock, R. Ravishankar, L. Van Looveren, P. A. Jacob, J. A. Martens, *J. Phys. Chem. B* **1999**, *103*, 4972.
[29] C. E. A. Kirschhock, R. Ravishankar, P. A. Jacobs, J. A. Martens, *J. Phys. Chem. B* **1999**, *103*, 11021.
[30] C. E. A. Kirschhock, V. Buschmann, S. Kremer, R. Ravishankar, C. J. Y. Houssin, B. L. Mojet, R. A. van Santen, P. J. Grobet, P. A. Jacobs, J. A. Martens, *Angew. Chem. Int. Ed.* **2001**, *40*, 2637.
[31] C. E. A. Kirschhock, S. P. B. Kremer, P. J. Grobet, P. A. Jacobs, J. A. Martens, *J. Phys. Chem. B* **2002**, *106*, 4897.
[32] S. Kremer, E. Theunissen, C. E. A. Kirschhock, P. A. Jacobs, J. A. Martens, W. Herfs, *Adv. Space Res.* **2003**, *32*, 259.
[33] C. E. A. Kirschhock, S. P. B. Kremer, J. Vermant, G. Van Tendeloo, P. A. Jacobs, J. A. Martens, *Chem. Eur. J.* **2005**, *11*, 4306.
[34] A. Aerts, L. R. A. Follens, M. Haouas, T. P. Caremans, M. A. Delsuc, B. Loppinet, J. Vermant, B. Goderis, F. Taulelle, J. A. Martens, C. E. A. Kirschhock, *Chem. Mater.* **2007**, *19*, 3448.
[35] T. M. Davis, T. O. Drews, H. Ramanan, C. He, J. S. Dong, H. Schnablegger, M. A. Katsoulakis, E. Kokkoli, A. V. McCormick, R. L. Penn, M. Tsapatsis, *Nat. Mater.* **2006**, *5*, 400.
[36] R. Ravishankar, C. Kirschhock, B. J. Schoeman, P. Vanoppen, P. J. Grobet, S. Storck, W. F. Maier, J. A. Martens, F. C. De Schryver, P. A. Jacobs, *J. Phys. Chem. B* **1998**, *102*, 2633.
[37] M. R. Baklanov, K. P. Mogilnikov, V. G. Polovinkin, F. N. Dultsev, *J. Vac. Sci. Technol. B* **2000**, *18*, 1385.

ADVANCED MATERIALS

[38] S. Eslava, M. R. Baklanov, C. E. A. Kirschhock, F. Iacopi, S. Aldea, K. Maex, J. A. Martens, *Langmuir* **2007**, *23*, 12811.
[39] P. I. Ravikovitch, A. Vishnyakov, A. V. Neimark, M. M. L. R. Carrott, P. A. Russo, P. J. Carrott, *Langmuir* **2006**, *22*, 513.
[40] E. Kondoh, M. R. Baklanov, E. Lin, D. W. Gidley, A. Nakashima, *Jpn. J. Appl. Phys. Part 2* **2001**, *40*, L323.
[41] J. N. Sun, D. W. Gidley, Y. F. Hu, W. E. Frieze, S. Yang, *Mater. Res. Soc. Symp. Proc.* **2002**, *726*, Q10.5.1.
[42] A. Grill, V. Patel, K. P. Rodbell, E. Huang, M. R. Baklanov, K. P. Mogilnikov, M. Toney, H. C. Kim, *J. Appl. Phys.* **2003**, *94*, 3427.
[43] D. W. Gidley, H. G. Peng, R. S. Vallery, *Annu. Rev. Mater. Res.* **2006**, *36*, 49.
[44] Z. J. Li, C. M. Lew, S. Li, D. I. Medina, Y. S. Yan, *J. Phys. Chem. B* **2005**, *109*, 8652.
[45] M. Johnson, Z. J. Li, J. L. Wang, Y. S. Yan, *Thin Solid Films* **2007**, *515*, 3164.